Thermochimica Acta, 115 (1987) 215–227
Elsevier Science Publishers B.V., Amsterdam – Printed in The Netherlands

SYNTHESIS OF γ-Fe_2O_3 BY THERMAL DECOMPOSITION OF $FeC_4H_2O_4 \cdot \frac{1}{2}H_2O$. PART II

A. VENKATARAMAN, V.A. MUKHEDKAR *, M.M. RAHMAN, A.K. NIKUMBH and A.J. MUKHEDKAR

Department of Chemistry, University of Poona, Pune 411 007 (India)

(Received 10 October 1986)

ABSTRACT

Thermal decomposition of ferrous fumarate half hydrate, $FeC_4H_2O_4 \cdot \frac{1}{2}H_2O$, has been investigated using direct current electrical conductivity, thermal analysis (simultaneous TGA, DTA and DTG), X-ray powder diffraction, infrared spectroscopy and gas chromatography techniques in static air, dynamic dry nitrogen and dynamic air.

The isothermal decomposition study of $FeC_4H_2O_4 \cdot \frac{1}{2}H_2O$ under different temperature ranges in all the above-mentioned atmospheres revealed the formation of anhydrous complex before its oxidative decomposition to α-Fe_2O_3 with the probable formation of intermediates of FeO, Fe_3O_4 and γ-Fe_2O_3 along with anhydrous complex.

Definite experimental conditions have been determined for the formation of γ-Fe_2O_3 in dynamic air containing water vapour by the use of direct current electrical conductivity measurements. γ-Fe_2O_3, thus obtained, has been characterized by X-ray diffraction, scanning electron microscopy, magnetic hysteresis measurements and Mössbauer spectroscopy.

INTRODUCTION

There has been a growing interest in the preparation of gamma ferric oxide (γ-Fe_2O_3), due to its technological importance as a magnetic tape recording material [1–5]. Commercially, γ-Fe_2O_3 is prepared from synthetic goethite (α-(FeO)OH) involving dehydration to α-Fe_2O_3, reduction to Fe_3O_4 and, finally, reoxidation to γ-Fe_2O_3 [6]. Recently, there are reports for the preparation of γ-Fe_2O_3 by thermal decomposition of ferrous oxalate dihydrate ($FeC_2O_4 \cdot 2H_2O$) [7,8] and ferrous succinate tetrahydrate ($FeC_4H_4O_4 \cdot 4H_2O$) [9]. However, the formation of γ-Fe_2O_3 during the decomposition of $FeC_4H_2O_4 \cdot \frac{1}{2}H_2O$ (ferrous fumarate half hydrate) has not been investigated so far. The present study investigates the thermal decomposition of ferrous fumarate half hydrate ($FeC_4H_2O_4 \cdot \frac{1}{2}H_2O$) by conventional thermal analysis (simultaneous TGA, DTG and DTA), supplemented with direct current

* Author for correspondence.

0040-6031/87/$03.50

electrical conductivity in the formation of γ-Fe_2O_3. The different steps involved during the thermal decomposition under static air, dynamic air, dynamic nitrogen and dynamic air containing water vapour will be discussed on the basis of results obtained systematically. The characterization of γ-Fe_2O_3 by X-ray powder diffraction scanning electron microscopy, magnetic measurements and Mössbauer spectroscopy will also be discussed.

EXPERIMENTAL

Apart from conventional solution chemistry precipitation techniques, various instrumental methods, such as IR spectra, C and H analysis, X-ray powder diffraction (XRD), thermal analysis (TGA, DTA and DTG), two-probe d.c. electrical conductivity, scanning electron microscopy (SEM), high field magnetic hysteresis loop tracer (HLT), initial magnetisation, Mössbauer spectroscopy and gas–liquid chromatography (GLC) are used.

The thermal analysis curves were recorded on a "NERTZ" instrument under static air, dynamic dry nitrogen and dynamic air atmospheres with a flow rate of nitrogen and dynamic air of 100 $cm^3\ min^{-1}$ and heating rates of, for the static air atmosphere, $5\,^\circ C\ min^{-1}$, and for the dynamic air and dynamic dry nitrogen atmospheres, $10\,^\circ C\ min^{-1}$. The d.c. electrical conductivity was measured on a Philips d.c. Micro Voltmeter PP 9004 instrument under static air, dynamic nitrogen, dynamic air and dynamic air containing water vapour [8] conditions. The heating rate was adjusted to $10\,^\circ C\ min^{-1}$ while the flow rate was maintained at 100 $cm^3\ min^{-1}$. The evolution of various gases during thermal decomposition of $FeC_4H_2O_4 \cdot \frac{1}{2}H_2O$ was recorded by Shimadzu RIA and Hewlet Packard instruments using nitrogen as the carrier gas. The morphology of γ-Fe_2O_3 particles was studied using a Cambridge Stereoscan 150 instrument. The XRD of samples were carried out in a Philips X-ray diffractometer (PW 1730) using MoK_α radiation. The magnetic properties were measured on a high field hysteresis loop tracer (HLT) and an initial magnetization unit [10]. Mössbauer spectra were taken on constant acceleration (Mössbauer spectrometer was assembled in the University's Department of Physics).

Preparation of $FeC_4H_2O_4 \cdot \frac{1}{2}H_2O$

$FeC_4H_2O_4 \cdot \frac{1}{2}H_2O$ was prepared by dissolving the metal carbonate in an aqueous solution of fumaric acid under a nitrogen atmosphere [11]. The values from the C and H analysis agreed with the calculated values within $\pm$ 0.4%. The IR spectrum had all the frequencies reported, and the XRD pattern proved that the sample was polycrystalline in nature with low symmetry. The half molecule of water of crystallization was confirmed on the basis of thermal analysis curves and d.c. electrical conductivity measurements.

RESULTS AND DISCUSSION

Static air atmosphere

The dehydration step of $FeC_4H_2O_4 \cdot \frac{1}{2}H_2O$ in Fig. 1a could be detected by the presence of a broad endothermic peak at 58 °C and also a broad peak at the same temperature on the DTG curve. However, the TGA curve showed continuous weight loss around this region, indicating that the anhydrous carboxylate ($FeC_4H_2O_4$) formed at this temperature is not stable with respect to temperature. The plot of log σ versus $1/T$ in Fig. 1b showed an increase in σ from 40 to 85 °C and a decrease up to 160 °C (region B) for the dehydration step. The isothermally heated $FeC_4H_2O_4 \cdot \frac{1}{2}H_2O$ sample under this atmosphere at 90 °C did not have any H–OH bands in the IR spectrum, however, the XRD pattern was similar to the parent compounds, i.e. crystalline in nature with a slight decrease in interplanar spacings. The elemental analysis agreed well with the anhydrous carboxylate formula: $FeC_4H_2O_4$.

The DTA curve in Fig. 1a had a very strong and broad exothermic peak at 290 °C, a broad peak at the same temperature, along with a hump at 395 °C, was observed on the DTG curve which corresponded to the oxidative decomposition of $FeC_4H_2O_4$. Due to the broadness of this peak the various intermediates formed during this step could not be detected, further,

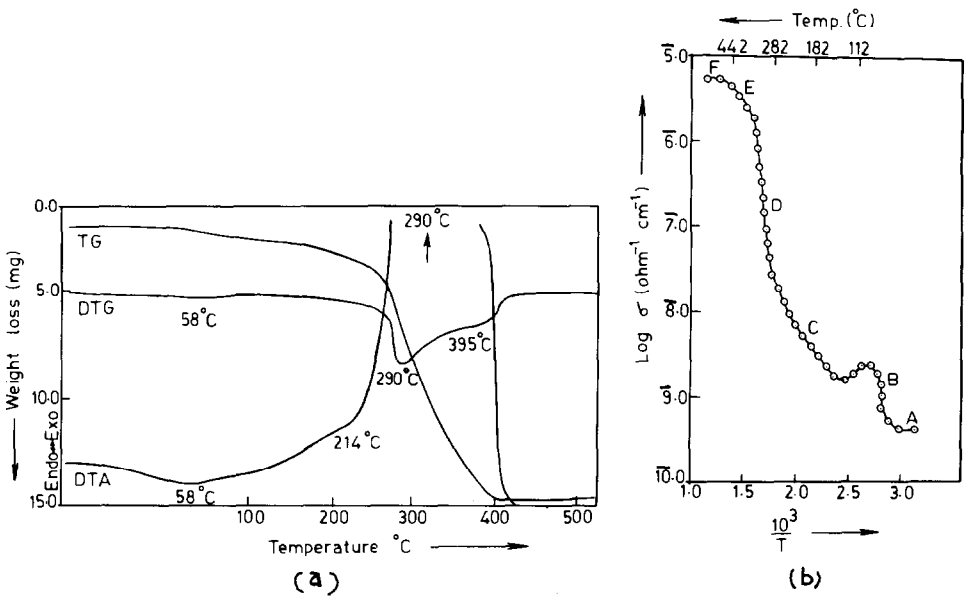

Fig. 1. Static air atmosphere: (a) thermal analysis curves (TGA, DTA, DTG) for $FeC_4H_2O_4 \cdot \frac{1}{2}H_2O$; (b) plot of log σ versus $1/T$ for $FeC_4H_2O_4 \cdot \frac{1}{2}H_2O$ or heating curve.

the TGA curve exhibited continuous weight loss until crystallization to α-Fe_2O_3 occurred.

The plot of log σ versus $1/T$ for $FeC_4H_2O_4 \cdot \frac{1}{2}H_2O$ shown in Fig. 1b had different values of conductivities corresponding to the various intermediates formed during the oxidative decomposition of $FeC_4H_2O_4$.

The σ value steadily increased from 160 to 326 °C (region C), and the IR spectrum of the isothermally heated $FeC_4H_2O_4 \cdot \frac{1}{2}H_2O$ sample at 320 °C showed a decrease in intensity of coordinated carboxylate bands, in addition, bands at 390 cm^{-1} (s) and 360 cm^{-1} (m) occurred for metal–oxygen stretching frequencies due to the presence of iron oxide [12]. The XRD pattern of this isothermally heated sample showed the structure to be polycrystalline in nature, and peaks corresponding to both $FeC_4H_2O_4$ and FeO were observed.

Although a tendency for a sharp increase in σ was observed at 330 °C (region D), the characteristic high value of Fe_3O_4 (3.0 Mho cm^{-1}) could not be obtained under dynamic conditions and a decrease in σ was seen at 395 °C (region E), probably due to the formation of semiconducting γ-Fe_2O_3. The sample in region E (360–420 °C) is mainly γ-Fe_2O_3 with traces of Fe_3O_4, the XRD was generally broad, having peaks corresponding mainly to γ-Fe_2O_3 and traces of Fe_3O_4. The IR spectrum of $FeC_4H_2O_4 \cdot \frac{1}{2}H_2O$, heated at 330 °C, showed no bands due to a coordinated carboxylate group, however, strong, broad bands, corresponding to Fe–O stretching frequencies, were observed. This part of the graph is followed by region F, i.e. above 441 °C, corresponding to the complete transformation of γ-Fe_2O_3 to α-Fe_2O_3.

When the reaction has been carried out using the normal atmosphere, the gaseous products act as a gas buffer for the solid state reaction and some of the reactions will be ill-defined. For example, the role of the half water molecule in $FeC_4H_2O_4 \cdot \frac{1}{2}H_2O$ and the role of atmospheric oxygen in the solid state reaction carried out in static air can be clarified by comparing the data of different physical properties for the same reaction carried out in a dynamic, dry nitrogen atmosphere.

Dynamic nitrogen atmosphere

The TGA curve for $FeC_4H_2O_4 \cdot \frac{1}{2}H_2O$ in Fig. 2a showed a clear dehydration step corresponding to the loss of the half water molecule from 80 to 108 °C, and this stage is supported by the presence of an endothermic peak at 94 °C on the DTA curve and a peak at 101 °C on DTG curve. The plot of log σ versus $1/T$ in Fig. 2b showed a clear peak at 100 °C corresponding to the dehydration step, the $FeC_4H_2O_4 \cdot \frac{1}{2}H_2O$ sample, heated isothermally under dynamic, dry nitrogen at 110 °C, showed no H–OH bands in the IR spectrum and the XRD pattern showed a decrease in interplanar spacing, which was similar to that obtained for the anhydrous carboxylate ($FeC_4H_2O_4$) under a static air atmosphere, given in Table 1. The decomposi-

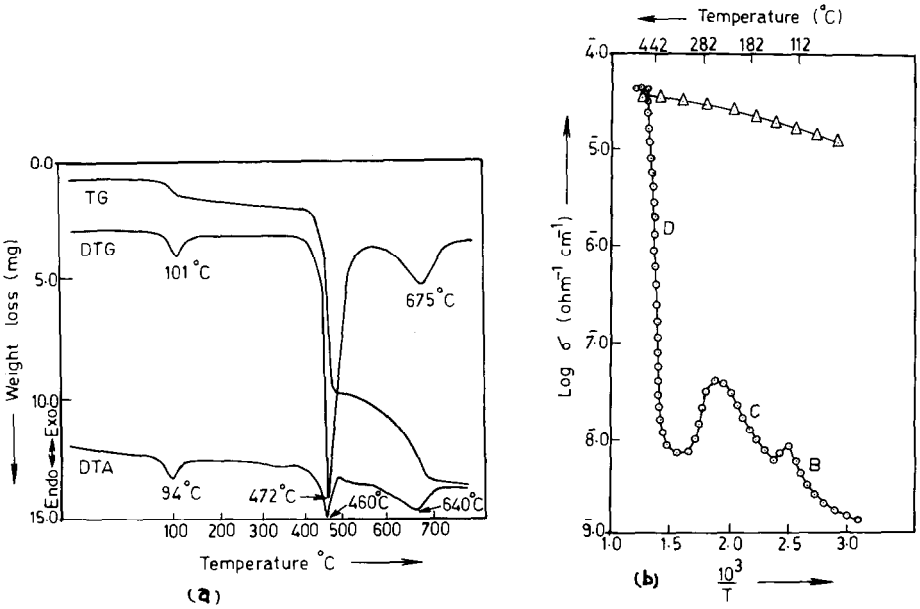

Fig. 2. Dynamic nitrogen atmosphere: (a) thermal analysis curves (TGA, DTA, DTG) for $FeC_4H_2O_4 \cdot \frac{1}{2}H_2O$; (b) plot of log σ versus $1/T$ for $FeC_4H_2O_4 \cdot \frac{1}{2}H_2O$ (△, cooling curve; ⊙, heating curve).

TABLE 1

XRD data of isothermally decomposed sample of $FeC_4H_2O_4 \cdot \frac{1}{2}H_2O$ under a dynamic nitrogen atmosphere

Observed *d*-spacing values of $FeC_4H_2O_4 \cdot \frac{1}{2}H_2O$ heated isothermally at 110 °C (Å)	Observed *d*-spacing values for $FeC_4H_2O_4 \cdot \frac{1}{2}H_2O$ heated isothermally at 330 °C (Å)	Observed *d*-spacing values for $FeC_4H_2O_4 \cdot \frac{1}{2}H_2O$ heated isothermally at 450 °C (Å)
3.838(w)		
3.508(w)	3.508	
3.407(m)	3.407(w)	3.407(w)
3.309(w)	3.309(w)	3.310(w)
2.984(w)	2.984(w)	
2.716(w)	2.716(w)	
2.686(w)	2.686(w)	
2.364(m)	2.364(m)	2.364(m)
2.052(s)	2.052(s)	2.052(s)
1.820(w)	1.821(w)	1.820(w)
1.748(w)	1.748(w)	
1.625(w)		

TABLE 2

XRD data of FeO and Fe_3O_4 obtained by isothermally heating $FeC_4H_2O_4 \cdot \frac{1}{2}H_2O$ under a nitrogen atmosphere

FeO (cubic) *d*-spacings observed by isothermally heating $FeC_4H_2O_4 \cdot \frac{1}{2}H_2O$ at 330 °C	Fe_3O_4 (cubic) *d*-spacings observed by isothermally heating $FeC_4H_2O_4 \cdot \frac{1}{2}H_2O$ at 450 °C
2.49(m)	4.850(w)
1.53(s)	2.967(m)
1.523(m)	2.530(s)
1.299(m)	2.093(m)
1.077(w)	1.609(m)
	1.275(w)
	1.091(w)
	0.967(w)
	0.880(w)
	0.812(w)

tion steps could be seen on the DTA curve at 460 °C (472 °C on the DTG curve) and crystallization to the α-Fe_2O_3 phase was observed at 642 °C on the DTA curve and 672 °C on DTG curve. The TGA curve showed weight loss from 342 to 460 °C and a further weight loss from 460 to 690 °C. However, the weight loss calculated from the TGA curve could not reveal the formation of any particular single intermediate species. The plot of log σ versus $1/T$ clearly showed the different intermediate phases which occurred during decomposition. Here, the cooling curve was also noted to test the purity of Fe_3O_4 formed. The sample obtained on isothermally heating $FeC_4H_2O_4 \cdot \frac{1}{2}H_2O$ in region C (330 °C) showed that the IR bands corresponding to Fe–O stretching frequencies increased, and those due to coordinated carboxylate bands decreased in intensity. The XRD pattern was similar to that of the isothermally heated sample under static air at 320 °C, indicating that the sample obtained was a mixture of FeO and some $FeC_4H_2O_4$ (Tables 1 and 2). The cooling curve of the sample at 440 °C was not completely that of a metallic semiconductor type [8,13]: it showed a decrease in the σ value, suggesting the presence of some compound with Fe_3O_4 (metallic semiconductor). The sample of $FeC_4H_2O_4 \cdot \frac{1}{2}H_2O$ isothermally heated at 450 °C under the same atmosphere showed weak coordinated carboxylate bands in the IR spectrum, the XRD pattern had peaks corresponding to mainly Fe_3O_4 with some $FeC_4H_2O_4$ (Tables 1 and 2). Thus, on the basis of IR, XRD and elemental analysis, it can be said that some $FeC_4H_2O_4$ was still present at this temperature, although the sample was mainly Fe_3O_4, and it can be tentatively suggested that the presence of $FeC_4H_2O_4$ causes a decrease in the σ value during cooling [14].

Although the nature of decomposition and final products obtained from static air and dynamic (dry and pure) nitrogen atmospheres for $FeC_4H_2O_4 \cdot \frac{1}{2}H_2O$ were similar, a few critical differences do exist, of which the major are:

(a) The TGA curve under dynamic nitrogen showed a clear weight loss with a plateau corresponding to a dehydration step, whereas a continuous weight loss was exhibited by the TGA curve under static air.

(b) The presence of some $FeC_4H_2O_4$ (anhydrous), along with Fe_3O_4, was observed under dynamic nitrogen, whereas no such observation was made under static air.

(c) Region E, corresponding to the γ-Fe_2O_3-formation stage, could not be identified under nitrogen, whereas this region could be detected under static air.

(d) The thermal analysis curves under nitrogen were resolvable, which corresponded with the observed changes in the log σ versus $1/T$ plots, whereas the thermal analysis curves under static air conditions were not clear.

Dynamic air atmosphere

In Fig. 3a, for $FeC_4H_2O_4 \cdot \frac{1}{2}H_2O$, the DTA and DTG curves had no resolvable peaks for the dehydration step, and the TGA curve showed continuous weight loss from room temperature until crystallization to α-Fe_2O_3. The broad exothermic peak corresponding to oxidative decomposi-

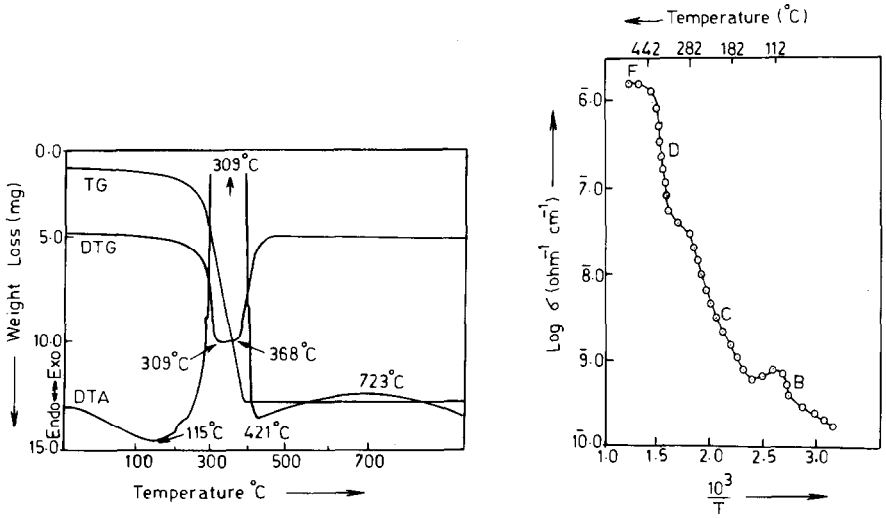

Fig. 3. Dynamic air atmosphere: (a) thermal analysis curves (TGA, DTA, DTG) for $FeC_4H_2O_4 \cdot \frac{1}{2}H_2O$; (b) plot of log σ versus $1/T$ for $FeC_4H_2O_4 \cdot \frac{1}{2}H_2O$ heating curve.

tion was shown on the DTA curve at 309 °C, a peak at this temperature was also seen on the DTG curve, and the TGA curve showed a continuous weight loss in this region. In general, the thermal analysis (TG, DTA and DTG) curves obtained were similar to Fig. 1a. The plot of log σ versus $1/T$ in Fig. 3b showed the dehydration peak at 110 °C, and the nature of the decomposition is similar to that shown in Fig. 1b. The isothermal decomposition under a dynamic air atmosphere for $FeC_4H_2O_4 \cdot \frac{1}{2}H_2O$ at various temperature regions showed that the products obtained were similar to those from isothermally decomposing $FeC_4H_2O_4 \cdot \frac{1}{2}H_2O$ under a static air atmosphere. The only difference using this atmosphere was that there was no formation of γ-Fe_2O_3.

These observations suggest that the solid state decomposition of $FeC_4H_2O_4 \cdot \frac{1}{2}H_2O$ under the buffer atmosphere in static air and in dynamic air follow slightly different patterns. Experimental data determined in dynamic air containing water vapour could provide further information on the solid state thermal decomposition of $FeC_4H_2O_4 \cdot \frac{1}{2}H_2O$.

Dynamic air atmosphere containing water vapour

Figure 4a shows the plot of σ versus $1/T$ for $FeC_4H_2O_4 \cdot \frac{1}{2}H_2O$.

The progress of decomposition of $FeC_4H_2O_4 \cdot \frac{1}{2}H_2O$ in this atmosphere (dynamic air containing water vapour), as studied by IR spectra, indicated

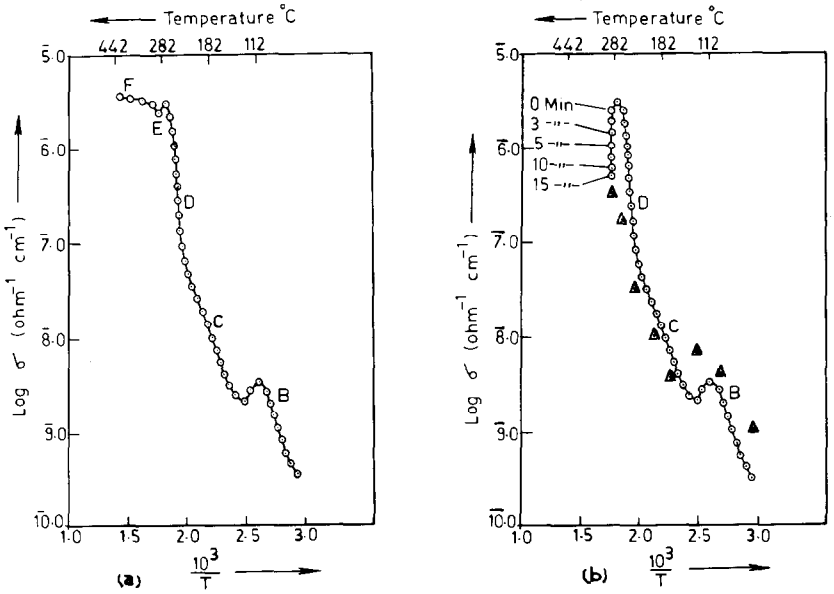

Fig. 4. Dynamic air atmosphere containing water vapour: (a) plot of log σ versus $1/T$ for $FeC_4H_2O_4 \cdot \frac{1}{2}H_2O$; (b) plot of log σ versus $1/T$ for $FeC_4H_2O_4 \cdot \frac{1}{2}H_2O$ (time dependent case) (⊙, heating curve; △, cooling curve).

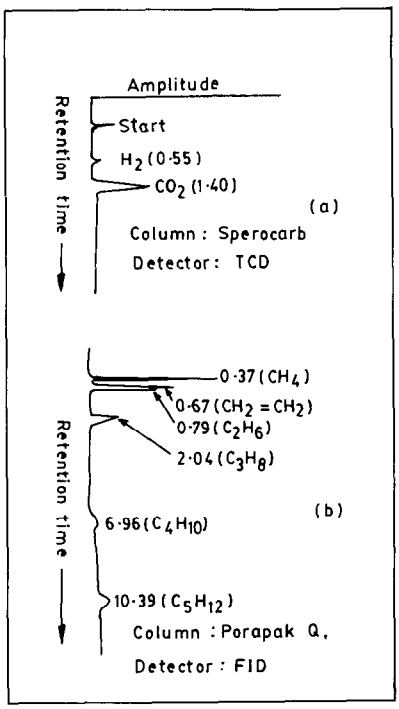

Fig. 5. Gas–liquid chromatograms for the gases obtained during the thermal decomposition of $FeC_4H_2O_4 \cdot \frac{1}{2}H_2O$ under a nitrogen atmosphere.

the formation of $FeC_4H_2O_4$ at 112 °C. A steep increase in σ value from 135 to 230 °C indicated the presence of a mixture of FeO and some $FeC_4H_2O_4$. This increase in σ was followed by a very steep increase from 235 to 270 °C before the sample underwent irreversible transformation into α-Fe_2O_3 at 400 °C. A well-resolved kink was observed at 290 °C. The step from 245 to 270 °C indicated the formation of Fe_3O_4. The IR spectral study and XRD pattern revealed that $FeC_4H_2O_4$ was stable up to 250 °C, along with Fe_3O_4, and from 250 to 270 °C only monophasic Fe_3O_4 was present. The well-resolved kink at 290 °C is characteristic of the formation of γ-Fe_2O_3 [8] and, above 395 °C, a complete irreversible transformation of α-Fe_2O_3 occurred.

A careful analysis of the time-dependent σ measurements in the temperature range 280–295 °C revealed the following points:

(a) There was no change in the σ value with variation of time up to 290 °C.
(b) At 290 °C the σ value changed from 6.50 to 8.75 Mho cm^{-1} within 15 min (Fig. 4b).
(c) There was no further decrease of σ above 295 °C.
(d) On further cooling the sample from 290 °C to room temperature the σ value fell, showing a maximum (Fig. 5, cooling cycle). The sample thus obtained was heated under a pure, dry nitrogen atmosphere at 200 °C to

TABLE 3

Literature XRD data for FeO and Fe_3O_4

FeO (cubic) *d*-spacing (ASTM, 6-615) (Å)	FeO (rhombohedron) *d*-spacing values (ASTM, 6-711) (Å)	Fe_3O_4 *d*-spacing values (ASTM, 19-629) (Å)
		4.850(8) [a]
		2.967(30)
		2.532(100)
2.490(80) [a]		2.424(8)
2.153(100)		2.099(20)
		1.715(10)
		1.616(30)
1.523(60)	1.525(100) [a]	1.485(40)
	1.512(100)	1.419(2)
		1.328(4)
1.299(25)	1.301(20)	1.281(10)
		1.266(4)
	1.236(60)	1.212(2)
		1.122(4)
		1.093(12)
1.077(15)	1.074(60)	1.050(6)
		0.9896(2)
		0.9695(6)
		0.9388(4)
		0.8952(2)
		0.8802(6)
		0.8569(8)
		0.8233(4)
		0.8117(6)
		0.8080(4)

[a] Figures in parentheses show the relative line intensities, normalized to that of the strongest intensity line (given by 100).

remove moisture. The XRD pattern of this sample showed it to be pure γ-Fe_2O_3 with a cubic configuration (Table 4) [15].

The predicted intermediates and products obtained at each temperature region under all the above atmospheres for $FeC_4H_2O_4 \cdot \frac{1}{2}H_2O$ are given in Table 5.

The gases obtained by thermally decomposing $FeC_4H_2O_4 \cdot \frac{1}{2}H_2O$ under a dynamic (dry and pure) nitrogen atmosphere are represented by the chromatograms shown in Fig. 5a,b. These chromatograms show the presence of both types of gases, i.e. polar (viz. CO, CO_2, H_2, etc.) and non-polar gases (viz. CH_4, C_2H_6, C_3H_8, etc.). The temperature of the gases collected was around 350 °C.

The high field HLT measurements at room temperature for γ-Fe_2O_3 in powder form showed the H_c value to be 250 Oe, the M_s value to be 70 emu

TABLE 4

XRD data of γ-Fe_2O_3 obtained from $FeC_4H_2O_4 \cdot \frac{1}{2}H_2O$

d (Å)	hkl	a_0 (Å)	Average a_0 (Å)
3.732	210	8.345	
3.420	211	8.377	
2.964	220	8.383	
2.529	311	8.387	
2.320	320	8.365	
2.220	321	8.306	
2.091	400	8.364	
1.710	422	8.377	
1.615	511/333	8.392	8.353
1.480	440	8.372	
1.310	620	8.285	
1.270	533	8.328	
1.200	444	8.314	
1.120	642	8.381	
1.090	553/731	8.372	
1.060	650	8.279	
1.040	652/740/810	8.384	

$a_0 = d(\sqrt{(h^2 + k^2 + l^2)})$

g^{-1} and the squareness ratio to be 0.55. All these values are in accordance with the room temperature theoretical values [16] for a single domain (SD) γ-Fe_2O_3 with the vacancy ordered configuration of Fe_8^{3+} $[Fe_{40/3}^{3+} \square_{8/3}]$ O_{32}.

TABLE 5

Predicted products formed during the decomposition of $FeC_4H_2O_4 \cdot \frac{1}{2}H_2O$

Atmosphere	Temperature ranges (°C)	Region	Predicted products
Static air	60–160(80) [a]	B	$FeC_4H_2O_4$
	160–326	C	$FeO + FeC_4H_2O_4$
	326–395	D	Fe_3O_4
	395–421	E	γ-Fe_2O_3
	> 421	F	α-Fe_2O_3
Dynamic dry nitrogen	65–160(110)	B	$FeC_4H_2O_4$
	160–280	C	$FeO + FeC_4H_2O_4$
	280–440	D	$Fe_3O_4 + FeC_4H_2O_4$
	> 440	F	α-Fe_2O_3
Dynamic air	60–160(102)	B	$FeC_4H_2O_4$
	160–309	C	$FeO + FeC_4H_2O_4$
	309–440	D	Fe_3O_4
	> 440	F	α-Fe_2O_3

[a] Figures in parentheses indicate the peak position.

Since γ-Fe_2O_3 is ferrimagnetic and α-Fe_2O_3 anti-ferromagnetic, initial susceptibility (X_i) measurements were employed to serve as a tool to obtain the Curie temperature (T_c). On the basis of X_i–T measurements, the Curie temperature (T_c) for the γ-Fe_2O_3 to α-Fe_2O_3 transformation occurred at 450 °C, further, these measurements revealed the SD behaviour for the γ-Fe_2O_3 sample before its transformation into α-Fe_2O_3 with a well defined Hopkinson's peak [17].

The SEM showed γ-Fe_2O_3 particles to be 1–2 μm in length and acicular in shape.

Six well resolved, narrow bands (half band width, 0.285 mm) in the intensity ratio 3 : 2 : 1 : 1 : 2 : 3 were observed in the Mössbauer spectrum (the value of the hyperfine field was found to be 498.8 $\pm$ 5.0 kOe, similar to that reported in the literature [18]).

CONCLUSION

The present study elucidated the following important points concerning the solid state decomposition of $FeC_4H_2O_4 \cdot \frac{1}{2}H_2O$ and the magnetic and Mössbauer properties of γ-Fe_2O_3 thus synthesized during the thermal decomposition of $FeC_4H_2O_4 \cdot \frac{1}{2}H_2O$:

(a) The XRD pattern showed $FeC_4H_2O_4 \cdot \frac{1}{2}H_2O$ to be polycrystalline in nature and with low symmetry.

(b) As the conventional thermal analysis curves (TGA, DTA, DTG) showed a very broad and strong exothermic peak (DTA curves), and a continuous weight loss in the TGA curves for the carboxylate under all atmospheres at the oxidative decomposition step, they could not give information regarding the type of intermediates formed. Hence, it was found necessary to supplement these results with more reliable techniques, i.e. use of d.c. electrical conductivity measurements, IR spectral investigations and XRD methods.

(c) The TGA curve under a dynamic nitrogen atmosphere showed a clear weight loss with a plateau corresponding to a dehydration step, whereas a continuous weight loss on the TGA curve was observed in static and dynamic air atmospheres.

(d) The final product of decomposition of $FeC_4H_2O_4 \cdot \frac{1}{2}H_2O$ under all atmospheres was α-Fe_2O_3.

(e) The gas chromatograms showed that both polar and non-polar gases were present during the thermal decomposition of $FeC_4H_2O_4 \cdot \frac{1}{2}H_2O$.

(f) The SEM, high field HLT and X_i–T measurements showed that the γ-Fe_2O_3 sample synthesized from $FeC_4H_2O_4 \cdot \frac{1}{2}H_2O$ possessed the required properties enabling it to behave as an efficient tape recording material.

ACKNOWLEDGEMENT

The authors are grateful for the financial assistance given by the Grants-in-aid (Defence Ministry), Government of India.

REFERENCES

1 W.P. Osmond, Proc. Soc. London B, 65 (1952) 121.
2 W.P. Osmond, Proc. Soc. London B, 66 (1953) 265.
3 W.P. Osmond, Proc. Soc. London B, 67 (1954).
4 J. Smit, Magnetic Properties of Materials, Inter-University Electronic Series, Vol. 13, McGraw-Hill, New York, 1971.
5 R.M. White, J. Appl. Phys., 57(1) (1985) 2996.
6 D.J. Craik, Magnetic oxides, Vol. II, Wiley Interscience, New York, 1975.
7 K. Seshan, H.R. Anantharaman, Venkatesh Rao, A.L. Shashimohan, H.V. Keer and D.K. Chakraborthy, Bull. Mater. Sci., 3 (1981a) 201.
8 K.S. Rane, A.K. Nikumbh and A.J. Mukhedkar, J. Mater. Sci., 16 (1981) 2387.
9 A. Venkataraman, V.A. Mukhedkar, M.M. Rahman, A.K. Nikumbh and A.J. Mukhedkar, Thermochim. Acta (in press).
10 S.D. Likhite, C. Radhakrishnamurthy and A.W. Sahasrabudhe, Rev. Sci. Instrum., 36 (1958) 1558.
11 C.P. Prabhakaran and C.C. Patel, Ind. J. Chem., 7 (1969) 266.
12 N.T. McDevitt and W.L. Baun, Spectrochim. Acta, 66 (1964) 255.
13 A. Demenicali, Phys. Rev., 78(4) (1950) 458.
14 A. Venkataraman, M.M. Rahman, A.K. Nikumbh, V.A. Mukhedkar and A.J. Mukhedkar, ICC University of Gorakhpur 1984 (Dec.), pp. 10, 15.
15 ASTM File number 24-81.
16 G. Bate, in D.J. Craik (Ed.), Magnetic Oxides, Vol. II, Wiley-Interscience, New York, 1975, p. 689.
17 C.R.K. Murthy, J. Geol. Survey India, 26 (1985) 640.
18 W.H. Kelly, V.J. Folen, M. Hass, W.N. Schreiner and G.B. Beard, Phys. Rev., 124 (1951) 80.